(ANPA Conference 2024)
ISSN: 2392-473X(Print), 2738-9537 (Online)

Research Article ©Nepal Physical Society
DOI: https://doi.org/10.3126/jnphyssoc.v10i1.72846

Preparation of Activated Carbon Based On *Buddleja Paniculata* As A Low-Cost Electrode Material for Supercapacitor Application

Sunil Koju,[1] Umesh Lawaju,[2] Omkar Khadka,[1] Ram Chandra Rai,[3] Mim Lal Nakarmi,[4] and Prakash Joshi[5, a)]

[1)]*Department of Physics, Amrit Science Campus, Tribhuvan University, Kathmandu, Nepal*
[2)]*Department of Physics, Patan Multiple Campus, Tribhuvan University, Lalitpur, Nepal*
[3)]*Department of Physics, SUNY Buffalo State, Buffalo, NY 14222, USA*
[4)]*Department of Physics, Brooklyn College and the Graduate Center of the City University of New York, Brooklyn, NY 11210, USA*
[5)]*Department of Physics, Bhaktapur Multiple Campus, Tribhuvan University, Bhaktapur, Nepal.*

[a)]*Corresponding author:Prakash.joshi@bkmc.tu.edu.np*

Abstract. In this study, carbon was prepared by carbonization of $ZnCl_2$ activated wood of *Buddleja Paniculata* at 700 °C and the activated carbon was used in the preparation of the electrodes of supercapacitors. Physical properties of the activated carbon were analyzed by using X-ray Diffraction (XRD), Raman spectroscopy, Fourier Transform Infrared Spectroscopy (FTIR), N_2 adsorption-desorption isotherms, Scanning Electron Microscopy (SEM), and Energy Dispersive X-ray Spectroscopy (EDS). These analyses revealed a high carbon concentration (96.7 %) and a dominant amorphous carbon in the sample. The calculated Brunaeur-Emmet-Teller (BET) surface area of activated carbon was 1326 m^2g^{-1} with a high volume of microporous structures. The electrochemical properties of the prepared supercapacitor electrodes using activated carbon were analyzed by cyclic voltammetry (CV) and galvanostatic charge-discharge (GCD) tests in a three-electrode system. They exhibited excellent electrochemical double layer capacitance (EDLC) behavior and a specific capacitance of 117.58 Fg^{-1} at 1 Ag^{-1}. The above investigation indicates that the activated carbon of *Buddleja Paniculata* can be a low-cost supercapacitor electrode material.

Received: August 25, 2024; **Revised**: October 24, 2024; **Accepted**: November 01, 2024

Keywords: Activated carbon, *Buddleja Paniculata*, Electrochemical double layer capacitance, Supercapacitor.

INTRODUCTION

Electric double-layer capacitors (EDLCs) are gaining tremendous attention as energy storage devices due to their high power density, fast charge-discharge ability, and long cycle life [1]. EDLCs store energy by gathering charges at the interface between the electrode surface and the electrolyte [2]. The surface texture of the electrode material such as surface area and porosity have a significant influence in the capacitive performance of EDLCs [3]. Materials with high surface area, hierarchical porosity, and excellent conductivity are preferred for the fabrication of high capacitance EDLCs [4]. Carbonaceous materials have above mentioned features and also offer additional characteristics such as chemical and thermal stability, easy accessibility, and processability [5], hence, they are widely used in EDLCs. Activated carbon [3,6–11], carbon black [12], graphene [13], carbon nanotubes [14], mesoporous carbon microspheres [15], and lampblack [16] have been explored as electrode materials for EDLCs. Among them, activated carbon is usually preferred because of its features like low cost, porous structure, and large surface area.

Activated carbons are generally prepared using carbon rich biomass precursors such as rice husk [17], cotton stalk [18], coffee beans [19], lapsi seed [20], corncobs [21], banana fibers [22], and so on. Physical activation and chemical activation methods are used to prepare activated carbon. Physical activation is performed in an oxidative reactor such as O_2, CO_2, or steam at an elevated temperature of 700-1200 °C whereas chemical activation involves impregnation of precursors by chemicals ($ZnCl_2$,

KOH, NaOH, H_3PO_4, etc.) and then carbonization at a relatively lower temperature [23]. The activated carbon obtained from physical activation method generally possesses a lower surface area than that obtained from chemical activation. Alhebshi et al.[24], prepared activated carbon using date palm fronds with both physical and chemical activation methods. The authors reported a higher specific capacitance value for the chemically activated carbon 125.9 F g^{-1} than for physically activated carbon 56.8 F g^{-1} at the current density of 1 A g^{-1}. Similarly, Taurbekov et al. [25], reported a higher specific capacitance value of 150 F g^{-1} for chemically activated carbon compared to 40 F g^{-1} for physically activated carbon derived from rice husk. The authors also reported a specific capacitance of 152 F g^{-1} vs 109 F g^{-1} for chemically activated carbon and physically activated carbon respectively, prepared from walnut shells. So, in this research activated carbon was derived from the wood of *Buddleja paniculate* by using a chemical activation method.

Buddleja paniculate is a deciduous shrub indigenous to Nepal, Bhutan, Northern India, Myanmar as well as the Chinese provinces of Guangxi, Guizhou, Hunan, Jiangxi, Sichuan, and Yunnan. It thrives in thick and open forests at elevations of 500–3000 m [26].The plant has social and cultural values among the Indigenous people of the Kathmandu Valley, hence, it is widely grown in the farmland and gardens in the Kathmandu Valley and hilly regions of Nepal. This plant has woody stems and branches, thus, the wood of this plant can be easily available for the preparation of activated carbon.

Initial raw materials chosen for the preparation of activated carbon have an important impact on the pore size distribution (PSD) and surface area due to the different lignocellulosic content [10,11,20] and hence affect the capacitive performance of EDLCs. Along with precursor, activating agent and activating temperature can also impact PSD and surface area of the activated carbon. In this research, $ZnCl_2$ was selected as an activating agent as it can produce a well-developed porosity and yield high carbon concentration [17]. At low activation temperatures, the activated carbon has low conductivity and at high activation temperatures, the carbon yield is low [4,27]. So, an intermediate activation temperature of 700 °C was selected to prepare activated carbon. The prepared activated carbon yielded high-purity carbon at 96.7 % purity and its supercapacitor electrode showed a specific capacitance of 117.58 F g^{-1} at 1 A g^{-1}. In our previous work, we prepared supercapacitor electrodes with activated carbon derived from coffee waste and reported a specific capacitance of 113.81 F g^{-1} at 1 A g^{-1} [28].

EXPERIMENTAL METHODS

Preparation of Activated Carbon

The synthesis method of the activated carbon followed in this research is similar to that reported elsewhere [20,28]. The clean branch wood of a locally found plant, *Buddleja Paniculata* was collected, washed and fine powder of the wood was obtained for the preparation of activated carbon. The fine powder of wood was filtered through a 0.35 mm sieve. The obtained powder was mixed with zinc chloride ($ZnCl_2$) solution in the ratio of 1:1 by mass for the activation and left for 24 hours. After activation of the precursor, it was dried in an oven overnight. Carbonization of the dry activated precursor was done in a tubular furnace in the inert Nitrogen atmosphere at the temperature of 700 °C for 4 hours to obtain activated carbon. The obtained carbon was ground into a fine powder and initially washed with 0.1 M hydrochloric acid (HCl) and then washed with deionized water several times until the acid was neutralized. The obtained carbon was then dried and used for the characterization and fabrication of the electrode.

Material Characterization

Study of the surface morphology of the activated carbon was carried out using scanning electron microscopy (SEM) and its elemental composition was determined from the EDS system in the SEM using the FEI Helios Nanolab 660 scanning electron microscope, Thermo Fisher Scientific, USA. The structural properties were studied by XRD analysis using the Rigaku MiniFlex 600 diffractometer with the Cu Kα source (λ = 1.54 Å). Raman spectroscopy was used to determine the relative portions of ordered and disordered carbons in the sample. Fourier Transform Infrared Spectroscopy (FTIR) of the sample was employed to determine the functional groups using PerkinElmer Spectrum IR. The surface area and pore size distributions of the sample were measured using Autosorb-1C, Quantachrome, USA.

Fabrication of activated carbon-based working electrode and electrochemical measurement

The mixture of 4 mg activated carbon, 0.5 mg carbon black, and 0.5 mg polyvinylidene fluoride (PVDF) (bought from Apollo Scientific) was ground in a mortar. Then, 200 µl of n-methyl pyroline (NMP) was added to disperse PVDF and was mixed properly in the mortar. The obtained mixture was then coated onto 1 cm^2 nickel foam

and dried at a temperature of 70°C overnight. Here, PVDF was added as a binder, and carbon black was added as a conductivity enhancer [10,28]. The dried activated carbon coated nickel foam was then soaked in a 3 M potassium hydroxide (KOH) solution overnight.
The Gamry Interface 1010E (Gamry Instrument, USA) was used to test the cyclic voltammetry (CV) and galvanometric charge discharge (GCD) of the activated carbon electrode. The electrochemical characterization was done by using an experimental setup of a three-electrode system. Here, activated carbon coated nickel foam acts as a working electrode, platinum wire was used as a counter electrode, and an Ag/AgCl electrode as a reference electrode. For the electrolyte, 3 M aqueous solution of KOH was used. The CV measurement was carried out in the potential range of -0.2 to -1 V at various scan rates. The GCD tests were performed at a current density from 1 Ag^{-1} to 5 Ag^{-1} in the voltage range from -1.1 V to 0 V. The specific capacitance of the electrodes was calculated from CV curves by using the formula [29],

$$C_{sp} = \frac{A}{2KmV}. \quad (1)$$

Where C_{sp} is the specific capacitance (F g^{-1}), A is the integrated area under the CV curve (A.V), k is the scan rate (Vs^{-1}), m is the mass of the activated carbon in the electrode (g), and ΔV is the potential window (V).

For GCD tests, the specific capacitance was calculated as [29],

$$C_{sp} = \frac{I\Delta t}{m\Delta V}. \quad (2)$$

Where C_{sp} is the specific capacitance (F g^{-1}), I is the current (A), Δt is the discharge time (s), m is the mass of the carbon in the electrode (g), and ΔV is the potential window (V).

Result and discussion

Characterization of material

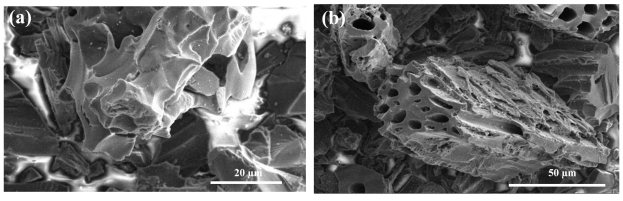

FIGURE 1. SEM image of activated carbon with (a) 1500 times magnification (b) 800 times magnification

Figure 1 illustrates the SEM images of the activated carbon sample. Figure 1(a) shows the irregular shaped fragmented particles with rough surface whereas Figure 1(b) shows the particles with micron-sized pores. The rough and porous morphology of the carbon ensured proper activation of the sample.

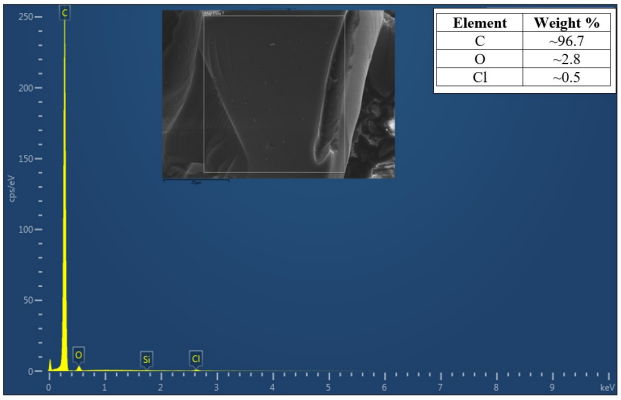

FIGURE 2. Energy dispersive X-rays spectroscopy spectrum (EDS) of activated carbon. The SEM image is displayed in the inset, and the EDS scanned area is indicated by a rectangle.

Figure 2 shows a typical EDS spectrum of the activated carbon sample. The spectrum indicates that the carbon sample contains approximately 96.7 % carbon, 2.8 % oxygen, and 0.5 % chlorine by weight in the typical scanned area. The presence of oxygen may be due to the remnants of different oxygen functional groups and the absorbed water vapor from the air in the sample. The presence of a small amount of chlorine could be due to the contamination of the sample.

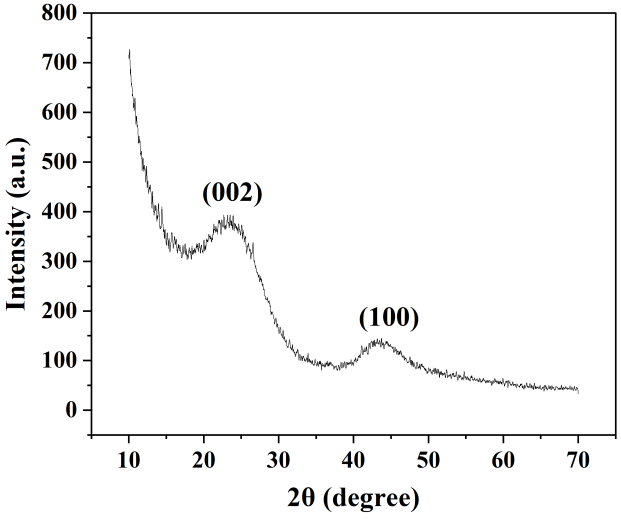

FIGURE 3. XRD pattern of activated carbon

Figure 3 represents the XRD profile for the activated

carbon sample. The two distinct broad peaks at angles $2\theta = 23.56^0$ and 43.74^0 correspond to the reflection from (002) and (100) planes of graphitic carbon, respectively [30]. Additionally, the XRD pattern shows a large background underlying the peaks. This indicates the existence of a significantly high fraction of amorphous carbon in the sample [31,32]. Hence, the activated carbon consists of graphitic carbon and dominant amorphous carbon [20].

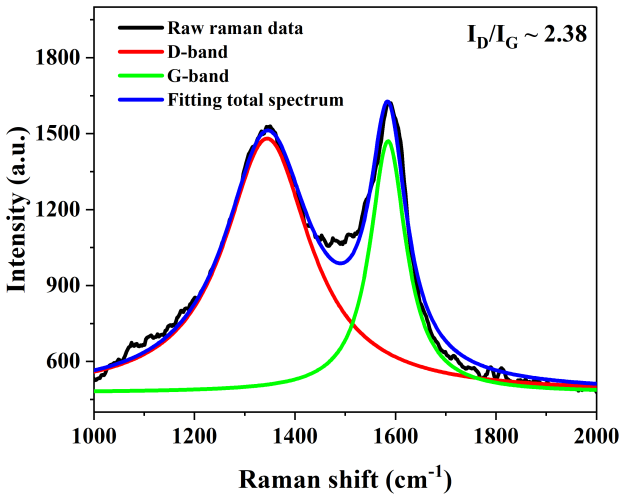

FIGURE 4. Raman spectrum of activated carbon. The coloured spectra represent the fitting of the raw data.

Figure 4 is the Raman spectrum of the activated carbon and it shows two typical adsorption bands of carbon at 1344 cm^{-1} and 1585 cm^{-1}, attributed to D-band and G-band, respectively [11,20,29]. The D-band corresponds to disordered carbon and the G-band corresponds to ordered graphitic layers [11,33]. Disordered carbon provides numerous active sites for ion adsorption and electrochemical reactions and ordered graphitic layers enhance electrical conductivity. However, it is believed that this improvement in conductivity comes at the cost of reducing the number of active sites [34–36]. The Raman spectrum is fitted using Lorentzian line shapes with background subtraction to calculate the portion of disordered and ordered carbon in the sample [37]. The intensity ratio of D and G bands, I_D/I_G, calculated by integrating the area under the corresponding peak is found to be 2.38. This indicates a very high content of amorphous carbon compared to the crystalline carbon in the sample [11]. This result is consistent with the result from the XRD pattern shown in Figure 3.

In the FTIR spectrum of the carbon sample shown in Figure 5, the broad peak centered around 3375 cm^{-1} is due to O-H stretching [10,38]. The peak at 2927 cm^{-1} and a small shoulder at 2851 cm^{-1} are associated with the symmetric and antisymmetric -C-H- stretching vibrations of CH_2 and CH_3 groups respectively [39]. The peak at 1541 cm^{-1} is due to N-O stretching of nitro compound [38].

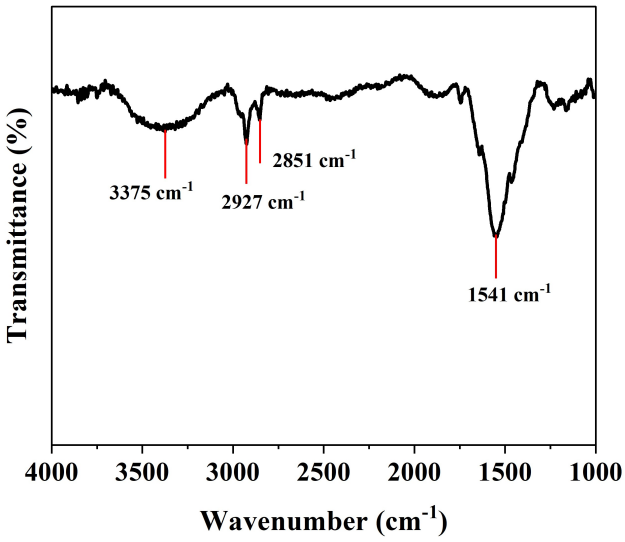

FIGURE 5. FTIR spectrum of activated carbon sample after background correction

The N_2 adsorption-desorption isotherm of the activated carbon, shown in Figure 6 is similar to the type I characteristics of microporous material [20]. Brunauer-Emmett-Teller (BET) surface area, micropore volume, pore width, and pore volume are listed in Table I. The specific surface area of the activated carbon was found to be 1326 m^2g^{-1}. The total pore volume obtained from the Density Func-

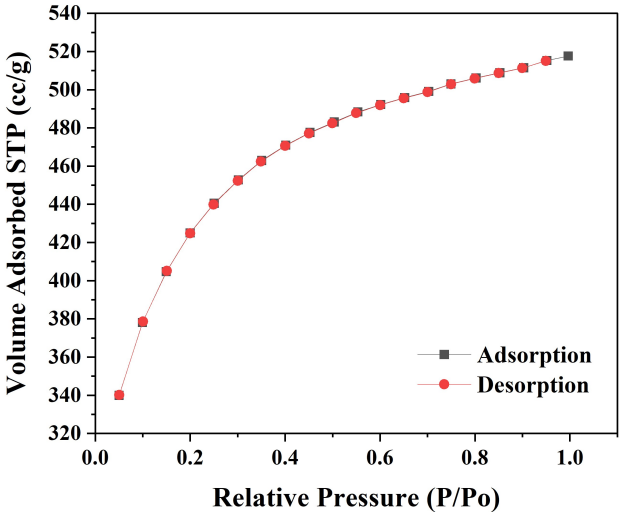

FIGURE 6. Nitrogen adsorption-desorption isotherm

tional Theory (DFT) method [40] is 0.7215 ccg^{-1} and micropore volume obtained from t-method [41] is 0.6144 ccg^{-1}. The maximum number of pores has a microporous width of 1.6134 nm validating the N_2 isotherm. The ratio of micropore area to the specific surface area is 89.21 %, which indicates a very high number of micropores in the sample.

TABLE I. : Specific surface area and pore characteristics of activated carbon

S_{BET} [a] (m^2g^{-1})	S_{micro} [b] (m^2g^{-1})	S_{micro}/S_{BET}	V_{micro} [c] (ccg^{-1})	W_{DFT} [d] (nm)	V_{DFT} [e] (ccg^{-1})
1326	1183	89.21%	0.6144	1.614	0.7215

[a] specific surface area.
[b] micropore area
[c] micropore volume using t-method
[d] pore width (mode) using DFT method
[e] pore volume using DFT analysis

Figure 7 show the pore size distribution obtained from the DFT method which indicates the presence of higher number of microporous structures with a pore size of about 1.61 nm. From the figure it can be seen that the activated carbon also contains a small volume of mesopores structures.

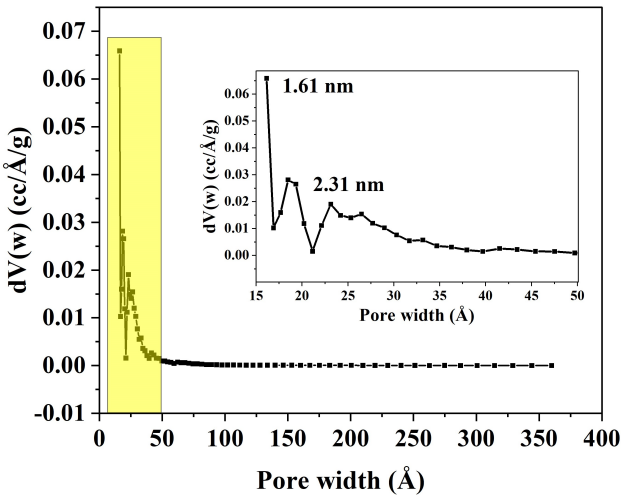

FIGURE 7. Pore size distribution obtained by the DFT method. The inset shows a close-up view of the shaded region.

Electrochemical properties

Cyclic voltammetry and galvanostatic charge-discharge (GCD) measurements were employed to evaluate the electrochemical properties and to calculate the specific capacitances of the electrode. CV of the prepared electrodes was tested in the potential window of -0.2 to -1 V in a three-electrode system. Figures 8(a) and 7(b) show CV curves recorded at 2 mVs^{-1} and multiple scan rates, respectively. At a low scan rate, 2 mVs^{-1}, the curve demonstrates a quasi-rectangular shape which shows the presence of both double layer capacitance and pseudo-capacitance. The pseudocapacitance is attributed to the redox reaction of functional groups in the carbon sample [6,42].

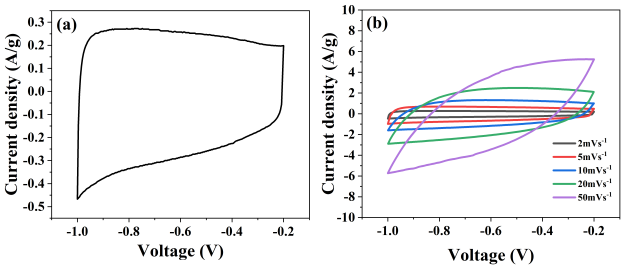

FIGURE 8. CV curves at (a) 2 mVs^{-1} and (b) different scan rates

Figure 8(b) shows the CV profile at different scan rates. At a high scan rate of 50 mVs^{-1}, the CV deviates from a typical rectangular shape and becomes sharp and tilted, indicating significant ohmic resistance in pores [43]. The specific capacitance for each scan rate was calculated using Equation 1. The specific capacitance at scan rates of 2, 5, 10, 20, and 50 mVs^{-1} is 128.79, 121.43, 100.98, 86.36 and 50.18 F g^{-1}, respectively. It is worth noting that the value of specific capacitance decreased as the scan rate increased. This characteristic result indicates the presence of micropores in the activated carbon which is consistent with the result obtained from N_2 adsorption-desorption analysis[44].

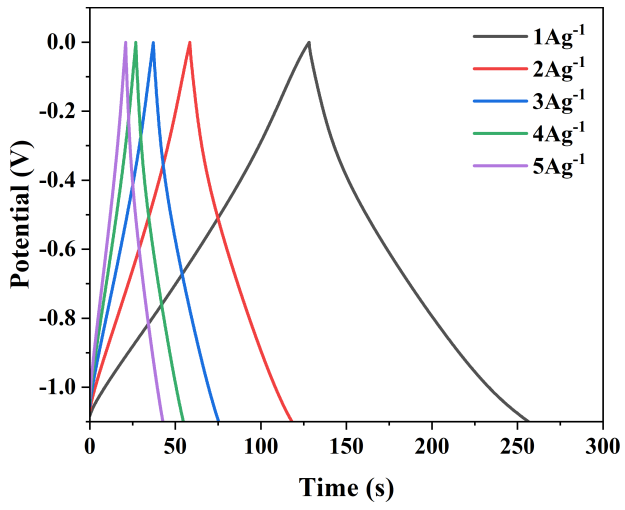

FIGURE 9. GCD curves at different current density

Figure 9 shows the GCD curves at different current

densities. The GCD curves are highly symmetric isosceles triangles suggesting good electrochemical reversibility and high Coulombic efficiency [45]. The specific capacitance, calculated using Equation 2, of the activated carbon electrode at the discharge rate 1, 2, 3, 4, and 5 A g^{-1} are 117.58, 109.62, 104.86, 102.11 and 99.64 F g^{-1}, respectively. So, there is only 15.3% decrease in capacitance when current density is increased from 1 to 5 A g^{-1}. This shows the high rate capability of the activated carbon electrode.

CONCLUSION

Supercapacitor electrodes prepared using activated carbon from the wood of *Buddleja Paniculata* exhibited excellent capacitive behavior and high rate capability. High surface area, high carbon content, and the presence of oxygen-containing functional groups in the *Buddleja Paniculata* based activated carbon contributed to its excellent electrochemical double layer capacitance (EDLC) behavior with specific capacitance of 117.58 F g^{-1} at the discharge rate of 1 A g^{-1}. These findings highlight the possibility of utilizing wood of *Buddleja Paniculata* to produce low-cost high-performance supercapacitor electrode material.

ACKNOWLEDGMENTS

The authors are thankful to Department of Physics, Amrit Science Campus (ASCOL), Tribhuvan University (T.U.), Bhaktapur Multiple Campus (BMC), T.U, Assoc. Prof. Sudarshana Shakya, BMC, Indian Institute of Technology, IIT-Kanpur, India and PSC- CUNY Grant, NY, USA for their support and cooperation.

EDITORS' NOTE

This manuscript was submitted to the Association of Nepali Physicists in America (ANPA) Conference 2024 for publication in the special issue of the Journal of Nepal Physical Society.

REFERENCES

1. R. Kötz and M. Carlen, "Principles and applications of electrochemical capacitors," Electrochimica acta **45**, 2483–2498 (2000).
2. B. E. Conway, "Electrochemical supercapacitors," 1st ed., Springer New York, NY (1999).
3. D. Qu and H. Shi, "Studies of activated carbons used in double-layer capacitors," Journal of Power Sources **74**, 99–107 (1998).
4. A. Ghosh and Y. H. Lee, "Carbon-based electrochemical capacitors," ChemSusChem **5**, 480–499 (2012).
5. E. Frackowiak and F. Beguin, "Carbon materials for the electrochemical storage of energy in capacitors," Carbon **39**, 937–950 (2001).
6. X. He, J. Lei, Y. Geng, X. Zhang, M. Wu, and M. Zheng, "Preparation of microporous activated carbon and its electrochemical performance for electric double layer capacitor," Journal of Physics and Chemistry of Solids **70**, 738–744 (2009).
7. O. Barbieri, M. Hahn, A. Herzog, and R. Kötz, "Capacitance limits of high surface area activated carbons for double layer capacitors," Carbon **43**, 1303–1310 (2005).
8. S. Yang and K. Zhang, "Converting corncob to activated porous carbon for supercapacitor application," Nanomaterials **8**, 181 (2018).
9. Y. Guo, T. Wang, X. Chen, and D. Wu, "Agar-based porous electrode and electrolyte for flexible symmetric supercapacitors with ultrahigh energy density," Journal of Power Sources **507**, 230252 (2021).
10. D. Shrestha, S. Maensiri, U. Wongpratat, S. W. Lee, and A. R. Nyachhyon, "Shorea robusta derived activated carbon decorated with manganese dioxide hybrid composite for improved capacitive behaviors," Journal of Environmental Chemical Engineering **7**, 103227 (2019).
11. A. A. Hor and S. Hashmi, "Optimization of hierarchical porous carbon derived from a biomass pollen-cone as high-performance electrodes for supercapacitors," Electrochimica acta **356**, 136826 (2020).
12. A. Krause, P. Kossyrev, M. Oljaca, S. Passerini, M. Winter, and A. Balducci, "Electrochemical double layer capacitor and lithium-ion capacitor based on carbon black," Journal of Power Sources **196**, 8836–8842 (2011).
13. C. Schütter, C. Ramirez-Castro, M. Oljaca, S. Passerini, M. Winter, and A. Balducci, "Activated carbon, carbon blacks and graphene based nanoplatelets as active materials for electrochemical double layer capacitors: a comparative study," Journal of the Electrochemical Society **162**, A44 (2014).
14. G. Wang, R. Liang, L. Liu, and B. Zhong, "Improving the specific capacitance of carbon nanotubes-based supercapacitors by combining introducing functional groups on carbon nanotubes with using redox-active electrolyte," Electrochimica Acta **115**, 183–188 (2014).
15. W. Xiong, M. Liu, L. Gan, Y. Lv, Y. Li, L. Yang, Z. Xu, Z. Hao, H. Liu, and L. Chen, "A novel synthesis of mesoporous carbon microspheres for supercapacitor electrodes," Journal of Power Sources **196**, 10461–10464 (2011).
16. U. Lawaju, K. Anupam, and P. Joshi, "Lampblack of soybean oil as a low-cost electrode material in supercapacitor application," Scientific World **16**, 94–99 (2023).
17. X. He, P. Ling, M. Yu, X. Wang, X. Zhang, and M. Zheng, "Rice husk-derived porous carbons with high capacitance by zncl2 activation for supercapacitors," Electrochimica Acta **105**, 635–641 (2013).
18. M. Chen, X. Kang, T. Wumaier, J. Dou, B. Gao, Y. Han, G. Xu, Z. Liu, and L. Zhang, "Preparation of activated carbon from cotton stalk and its application in supercapacitor," Journal of solid state electrochemistry **17**, 1005–1012 (2013).
19. T. E. Rufford, D. Hulicova-Jurcakova, Z. Zhu, and G. Q. Lu, "Nanoporous carbon electrode from waste coffee beans for high performance supercapacitors," Electrochemistry Communications **10**, 1594–1597 (2008).
20. L. K. Shrestha, R. G. Shrestha, S. Maji, B. P. Pokharel, R. Rajbhandari, R. L. Shrestha, R. R. Pradhananga, J. P. Hill, and K. Ariga, "High surface area nanoporous graphitic carbon materials derived from lapsi seed with enhanced supercapacitance," Nanomaterials **10**, 728 (2020).
21. D. Wang, Z. Geng, B. Li, and C. Zhang, "High performance electrode materials for electric double-layer capacitors based on

biomass-derived activated carbons," Electrochimica Acta **173**, 377–384 (2015).
22. V. Subramanian, C. Luo, A. M. Stephan, K. Nahm, S. Thomas, and B. Wei, "Supercapacitors from activated carbon derived from banana fibers," The Journal of Physical Chemistry C **111**, 7527–7531 (2007).
23. L. Miao, Z. Song, D. Zhu, L. Li, L. Gan, and M. Liu, "Recent advances in carbon-based supercapacitors," Materials Advances **1**, 945–966 (2020).
24. N. A. Alhebshi, N. Salah, H. Hussain, Y. N. Salah, and J. Yin, "Structural and electrochemical properties of physically and chemically activated carbon nanoparticles for supercapacitors," Nanomaterials **12**, 122 (2021).
25. A. Taurbekov, A. Abdisattar, M. Atamanov, M. Yeleuov, C. Daulbayev, K. Askaruly, B. Kaidar, Z. Mansurov, J. Castro-Gutierrez, A. Celzard, *et al.*, "Biomass derived high porous carbon via co_2 activation for supercapacitor electrodes," Journal of Composites Science **7**, 444 (2023).
26. A. J. M. Leeuwenberg, "The loganiaceae of africe xviii buddleja l. ii. revision of the african and asiatic species," Tech. Rep. (Landbouwhogeschool, 1979).
27. N. Bouchemal, M. Belhachemi, Z. Merzougui, and F. Addoun, "The effect of temperature and impregnation ratio on the active carbon porosity," Desalination and water treatment **10**, 115–120 (2009).
28. O. Khadka, U. Lawaju, S. Koju, R. C. Rai, M. L. Nakarmi, and P. Joshi, "Activated carbon derived from coffee waste as supercapacitor electrode material," Scientific World **17**, 19–26 (2024).
29. G. Singh, M. Sharma, A. Mathur, A. Halder, and R. Vaish, "Diesel soot as a supercapacitor electrode material," Journal of The Electrochemical Society **168**, 050551 (2021).
30. S. Singh, P. K. Bairagi, and N. Verma, "Candle soot-derived carbon nanoparticles: an inexpensive and efficient electrode for microbial fuel cells," Electrochimica Acta **264**, 119–127 (2018).
31. D.-S. Kang, S.-M. Lee, S.-H. Lee, and J.-S. Roh, "X-ray diffraction analysis of the crystallinity of phenolic resin-derived carbon as a function of the heating rate during the carbonization process," Carbon letters **27**, 108–111 (2018).
32. L. Lu, V. Sahajwalla, C. Kong, and D. Harris, "Quantitative x-ray diffraction analysis and its application to various coals," Carbon **39**, 1821–1833 (2001).
33. P. Joshi, "Novel counter electrodes of dye-sensitized solar cells based on activated carbon prepared from wood of choerospondias axillaris seed-stones and alnus nepalensis plant," Int. J. Eng. Adv. Res. Technol **3**, 8–11 (2017).
34. Y. Miyata, K. Mizuno, and H. Kataura, "Purity and defect characterization of single-wall carbon nanotubes using raman spectroscopy," Journal of Nanomaterials **2011**, 786763 (2011).
35. Y. Liu, X. Wang, X. Jiang, X. Li, and L. Yu, "Shape-controlled synthesis of porous carbons for flexible asymmetric supercapacitors," Nanoscale **10**, 22848–22860 (2018).
36. Y.-H. Chiu and L.-Y. Lin, "Effect of activating agents for producing activated carbon using a facile one-step synthesis with waste coffee grounds for symmetric supercapacitors," Journal of the taiwan institute of chemical engineers **101**, 177–185 (2019).
37. K. Anupam, J. Anderson, A. Ayala, C. Engdahl, E. L. Piner, and M. W. Holtz, "Heterogeneous integration of high-quality diamond on aluminum nitride with low and high seeding density," Journal of Crystal Growth **610**, 127172 (2023).
38. CHUNLIWANG991, "Ftir functional group database table with search - instanano," https://instanano.com/all/characterization/ftir/ftir-functional-group-search/.
39. M. A. Pantoja-Castro and H. González-Rodríguez, "Study by infrared spectroscopy and thermogravimetric analysis of tannins and tannic acid," Revista latinoamericana de química **39**, 107–112 (2011).
40. C. Lastoskie, K. E. Gubbins, and N. Quirke, "Pore size distribution analysis of microporous carbons: a density functional theory approach," The journal of physical chemistry **97**, 4786–4796 (1993).
41. J. De Boer, B. Lippens, B. Linsen, J. Broekhoff, A. Van den Heuvel, and T. J. Osinga, "Thet-curve of multimolecular n2-adsorption," Journal of colloid and interface science **21**, 405–414 (1966).
42. M. Karnan, K. Subramani, P. Srividhya, and M. Sathish, "Electrochemical studies on corncob derived activated porous carbon for supercapacitors application in aqueous and non-aqueous electrolytes," Electrochimica Acta **228**, 586–596 (2017).
43. T. Cai, M. Zhou, D. Ren, G. Han, and S. Guan, "Highly ordered mesoporous phenol–formaldehyde carbon as supercapacitor electrode material," Journal of Power Sources **231**, 197–202 (2013).
44. W. Xing, S. Qiao, R. Ding, F. Li, G. Lu, Z. Yan, and H. Cheng, "Superior electric double layer capacitors using ordered mesoporous carbons," Carbon **44**, 216–224 (2006).
45. M. Nazhipkyzy, G. Kurmanbayeva, A. Seitkazinova, E. A. Varol, W. Li, B. Dinistanova, A. Issanbekova, and T. Mashan, "Activated carbon derived from cucumber peel for use as a supercapacitor electrode material," Nanomaterials **14**, 686 (2024).